Crystallisation in flow Part II: Modelling crystal growth kinetics controlled by boundary layer thickness

Stanislas Sizaret [a,b*], Ivan Fedioun [c], Luc Barbanson [b], Yan Chen [b]

[a] Physico-chemical Geology, K.U. Leuven, Celestijnenlaan 200C, B-3001 Heverlee, Belgium

[b] ISTO, Université d'Orléans, 45067 Orléans cedex 02, France

[c] LCSR/CNRS 1c, avenue de la Recherche Scientifique, 45071 Orléans cedex 02, France

[*] Corresponding author

E-mail address: Stanislas.Sizaret@univ-orleans.fr (S.Sizaret)

SUMMARY

As in several other AMS studies, the main direction of the magnetic lineation analysed in Part I of this work, as well as crystal elongation, have been found to be roughly aligned with the direction of the surrounding flow. In order to explain the mechanisms responsible for such crystal shape anisotropy in a hydrodynamic context, we derive a mathematical model based on Falkner-Skan self-similar boundary layers at high Reynolds numbers. The model allows calculating local growth rates out of diffusion processes in the concentration boundary layer for crystal faces orientated arbitrarily in the range 90° to –18° with respect to the flow direction, and for any flow velocity. Hence, our work generalizes rationally previous attempts already done in the case of a flow parallel to the crystal face. This crystal growth model is applied to a natural case of calcite growth rate in 2D section perpendicular to the <c> axis. The reconstructed calcite growth reproduces the texture of a natural case observed in Part I, although the local Reynolds numbers are quite low. This approach may be applied for various geological settings, from deep

metasomatism to flowing on the earth surface.

Key words: fluid dynamics, crystallography, petrography

1 INTRODUCTION

In order to understand the relationship between Anisotropy of Magnetic Susceptibility (AMS) and mineral texture in a hydrodynamic context, a multidisciplinary study was carried out (Sizaret et al., Part I, 2006) on a well-known pipe-formed calcite. The AMS measurement on the magnetite-bearing calcite shows a good coherence between the magnetic lineation and the flow direction. However, the texture analyses by optical and imaging observations reveal two statistically distinguished directions which are about 15° slightly and oppositely misaligned with the fluid circulation direction. This consequently leads us to find a theoretical explanation at the crystal scale, based on crystal growth processes.

The idea that mineral shapes and textures are related to their intrinsic properties and to the influence of the external media is not new: Curie (1908) stated that "a crystal under an external influence will exhibit only those symmetry elements that are common to the crystal without the influence and to the influence without the crystal". Hence, in the case of crystal genesis in a flowing solution, the texture should be related to the surrounding flow field. Models describing crystal growth have been developed in different ways, both from experimental observations and from hydrodynamic considerations (e.g. Lebedev 1967; Kostov & Kostov 1999; Sizaret *et al.* 2006, Part I).

Experiments considering the bulk crystal shape showed that in case of volume diffusion, the bulk crystal growth rate is proportional to the square root of the flow velocity (Garside *et al.* 1975). Observations of growth bands in natural galena (Kessler *et al.* 1972) suggested that

upstream crystal faces possess a higher growth rate, which has been confirmed by experiments on ammonium-dihydrogen phosphate (ADP) (Prieto & Amoros 1981; Prieto et al. 1996). Chernov proposed a model to describe the processes of perturbation occurring on the crystal face at kink step scale by step bunching. In this model, the local flow is only considered in the vicinity of the mineral: it is parallel to the crystal face and increases exponentially from zero at the wall to a constant value at infinity, the variations of the velocity along the crystal face being neglected at this scale (Chernov 1992 and 2004).

The first attempts to establish a quantitative link between the crystal growth rate and the fluid velocity were limited to the case of a crystal face parallel to the flow (Carlson 1958; Gilmer *et al.* 1971; Rosenberger 1979). Gilmer *et al.* developed a unified formulation describing crystal growth rates by considering two kinds of processes: diffusion of solute through a volume of liquid (nearly) at rest relatively to the crystal surface, and reactions at the surface leading to the incorporation of molecules in the lattice. More recently, Prieto *et al.* (1996) considered three orientations: normal facing to the flow, parallel to the flow and in downstream position or '*in the shade*'. In the two previous cases, the authors invoked the classical hydrodynamic boundary layer theory to account for mass transfer through the '*concentration boundary layer'*, although eq. (3)-(6) in Prieto *et al.* (1996, p. 991) are questionable. In the "shade" position, experiments show lower growth rate: the crystal growth is perturbed, and step bunching process dominate in an eddy zone whose features depend on the flow velocity. In this latter case, the crystal face is in a wake flow, difficult to model from the hydrodynamic point of view, but in which the fluid may be considered nearly at rest, and for which the boundary layer theory is no longer valid.

Following these ideas, the aim of this paper is to develop a general model, based on rigorous self-similarity boundary layer analysis, to predict quantitatively crystal growth rates for arbitrary orientations of the faces, hence accounting for the observed asymmetry. The paper is

organized as follows: Section 2 recalls how crystal growth is related to diffusion processes, mainly to a concentration thickness Δ_c - the crux of the model- which has to be properly defined. Since readers of GJI are not familiar with the concept of boundary layers, the main elements of the theory are explained in section 3. The full model for Δ_c is given in section 4, and the major parameters controling the crystal growth are discussed in section 5. Results of the model are shown in section 6 in comparison with previous experimental work (Garside *et al.* 1975; Hilgers & Urai 2002) and are applied to reconstruct natural textures observed in Part I of this study (Sizaret *et al.* 2006, Part I).

2 CRYSTAL GROWTH EQUATION

Crystal growth modelled by Gilmer *et al.* (1971) is based on three differential equations describing mass balance at the three stages of crystal growth: (i) volume diffusion through the surrounding fluid towards the crystal surface, (ii) passage from volume to surface, (iii) diffusion along the surface and incorporation of adsorbed elements in kink sites (Fig. 1).

Figure 1

Assuming that $x_s << \Lambda$ (see below for definition), Gilmer *et al.* (1971) deduced the mathematical expression for the growth rate:

$$R = \frac{N_0 \Omega D \sigma}{\Lambda + \delta + \Lambda\Lambda_s \frac{y_0}{x_s^2} + \Lambda\left(\frac{y_0}{2x_s}\coth\left(\frac{y_0}{2x_s}\right) - 1\right)} \quad (1)$$

where R (m/s) is the growth rate, D (m^2/s) is the diffusion coefficient of ions in the solution, Λ is the distance defining the kinetics of adsorption of solute (i.e. drift velocity = D/Λ), Λ_s is the

distance defining the kinetics of incorporation of adsorbed solute in the step site (i.e. D_s/Λ_s , D_s being the diffusion coefficient along the crystal surface), x_s is the mean diffusion distance for adsorbed solute along the crystal surface, y_0 the average distance between two steps: in the Burton-Cambrera-Frank theory, this length is inversely proportional to the super-saturation (Burton *et al.* 1951). N_0 is the concentration of constitutive units in the solution, Ω the volume of a constitutive unit in the crystal, σ the relative super-saturation. The previous condition: $x_s << \Lambda$ is justified as the catchments length of constitutive units should be lower than the distance to enter the adsorption layer on crystal surface. The concentration boundary layer thickness δ that appears at the denominator of (1) is, however, not clearly defined, and attempt is done in this paper to fix this point.

Equation (1) can be simplified in the case where external conditions dominate the crystal growth, i.e. when the surface processes of incorporation of elements in the lattice are much faster than the feeding in elements by the solution. Consequently, internal parameters of the model should be negligible:

(i) $\Lambda << \delta$: the drift velocity D/Λ of solute molecules entering the adsorbed layer and

(ii) $\Lambda_s << x_s$: the drift velocity D_s/Λ_s of constitutive units passing from surface to steps are both higher than the volume diffusion velocity D/δ

(iii) $\delta/\Lambda >> y_0/2x_s$: the mean distance of superficial diffusion x_s is more than half of the distance y_0 between two steps i.e. the crystal face is not rough (there is a small number of steps on the face).

Therefore, under these conditions, and introducing the diffusion thickness Δ_c of our model, the general growth rate expression (1) can be reduced to:

$$R = \frac{N_0 \Omega D_{v.dif} \sigma}{\Delta_c} \qquad (2)$$

However, due to the uncertainty in the estimation of the parameters Λ, Λ_s, x_s and y_0, the balance between diffusion and surface processes cannot be known *a priori*. Hence, only an *a posteriori* analysis of the final crystal shape can indicate the prevailing process during the crystal growth. Again, from the Curie principle, asymmetric effects result from asymmetry in their cause. Thus, in each case where a uniform flow solution having a conical symmetry with infinite rotation axis (∞m) is the dominant driving force, the shape of a single crystal will show a symmetry breakdown: the shape formed under the influence of the flow has no centre of symmetry anymore. Upstream and downstream faces are not equivalent and should display different shapes, as observed on the natural calcite of the Chaudes-Aigues pipe shown in Part I. This remark could be helpful to distinguish hydrothermal texture from purely tectonic ones: the pure shear and simple shear deformations exhibit a centre of symmetry that flow processes do not reveal. Furthermore, the analysis of geological settings can give insight on possible occurrence of flowing solutions.

3 NEAR-WALL CRYSTAL HYDRODYNAMICS

Let us consider a crystal immersed in a flowing solution with (constant) velocity U_∞ and concentration c_∞. At the crystal surface, the fluid velocity is zero due to viscosity, and rapid incorporation of solute in the crystal maintains the wall concentration c_w constant, close to the saturation level and depending on the crystal solubility. This hypothesis supposes that no perturbation occur on the crystal face (Chernov, 1992). The crystal geometry is simplified in a 2D description within a horizontal plane perpendicular to two faces. The effects of gravity are

neglected. In that plane the crystal is assimilated to a 2D wedge (Fig. 2) to which a Cartesian coordinate system (x, y) is attached. The *x*-coordinate is measured along the crystal face from the leading edge (or the apex of the face), and the *y*- coordinate is normal to the wall. The angle between the flow direction and the *x* axis is $\beta \frac{\pi}{2}$: cases $\beta = 0$ (resp. $\beta = 1$) correspond to a flow parallel (resp. perpendicular) to the crystal face, reported in (Prieto *et al.* 1996). We deal here with an arbitrary orientation of the flow. At a given location *x*, leaving the surface along the *y*-coordinate, one observe a velocity profile $u(x, y)$ and a concentration profile $c(x, y)$ (Fig. 2). The velocity component *u* parallel to the face (*v* is the component perpendicular to the face, $v << u$) increases from zero at the wall to an outer velocity $U^e(x) \neq U_\infty$ if $\beta \neq 0$ depending on the orientation of the face in the flow and on the distance *x* measured from the leading edge along the crystal face. The concentration profile varies sharply from c_w to c_∞ as growth units are quickly incorporated in the crystal. Obviously, the concentration thickness Δ_c in (2) must be defined from the concentration profile $c(x, y)$ as a local value, i.e. $\Delta_c = \Delta_c(x)$, and the concentration profile itself depends on the velocity profile. Hence, hydrodynamics and crystal growth rate are closely related in a way detailed hereafter, which falls into the very classical theory of hydrodynamic boundary layer (e.g. Schlichting 1968).

Figure 2

First, let define the local hydrodynamic boundary layer thickness $\delta_H(x)$ as the height where the *u*-velocity reaches, say, 99% of U^e: $\delta_H(x) = y\big|_{u=0.99U^e}$. In the same way, one can define a concentration boundary layer thickness (not to be confused with Δ_c !) $\delta_c(x) = y\big|_{c=0.99c_\infty}$ (Fig.2). It

is easy to show by dimensional analysis that $\delta_H^2(x) \approx x\nu / U^e(x)$ and that $\delta_c^2(x) \approx xD / U^e(x)$, where $\nu = \mu / \rho$ and D are the momentum and mass diffusivities (m^2/s) in the flow. Thus, $\delta_H(x) \approx x\,\mathrm{Re}_x^{1/2}$ where $\mathrm{Re}_x = xU^e(x)/\nu$ is the local Reynolds number, and $\delta_H / \delta_c \approx Sc^{1/2}$ where $Sc = \nu / D$ is the Schmidt number of the solute in the flowing fluid (e.g. Evans 1961). If the Schmidt number is much higher than unity, it is expected that the concentration boundary layer will be thinner than the hydrodynamic boundary layer. These considerations are valid if the boundary layer is *laminar* (by opposition to *turbulent*), which is most probable since the local Reynolds number is unlikely to reach 10^4, the currently accepted value for laminar/turbulent transition. The set of PDEs describing the flow with high Reynolds number (i.e. $1 << \sqrt{\mathrm{Re}_x}$) in the wall-fitted coordinate system (x, y) is Prandtl equations together with the transport equation for the concentration:

$$\frac{\partial u}{\partial x} + \frac{\partial v}{\partial y} = 0 \qquad (3a)$$

$$u\frac{\partial u}{\partial x} + v\frac{\partial u}{\partial y} = U^e\frac{dU^e}{dx} + \nu\frac{\partial^2 u}{\partial y^2} \qquad (3b)$$

$$u\frac{\partial c}{\partial x} + v\frac{\partial c}{\partial y} = -\frac{\partial J}{\partial y} \qquad (3c)$$

with boundary conditions at the wall and outside the boundary layer:

$y = 0$: $u = v = 0$; $c = c_w$ and $y \to \infty$: $u \to U^e$; $c \to c_\infty$

In equation (3c), the mass flux is given by Fick's law: $J(x, y) = -D\frac{\partial c}{\partial y}$. It has been assumed that the concentration is small enough for the density ρ of the solution to be constant, so that eq. (3ab) and (3c) are uncoupled. This allows to solve the flow equations (3ab) for the velocity distribution $u(x, y)$ and $v(x, y)$, and to plug the result into (3c) which becomes linear with respect to the

unknown concentration distribution $c(x, y)$.

Let focus on the hydrodynamic problem. It appears that the kind of wedge flow we are interested in falls into a class of so-called *self-similar flows*, analysed by Falkner and Skan (see Schlichting 1968). This means that any velocity profile $u(x, y)$ has the same shape when described in terms of the single similarity variable $\eta = y / \Delta(x)$ where $\Delta(x)$ is some suitable thickness-scale to be defined (Fig. 3).

Figure 3

It is not useful to enter into the details here, but just give the result: the change in variable $u(x, y) = U^e(x) f'(\eta)$, $v(x, y) = U^e(x)\Delta'(x)\left(\eta f' - f\right) - \Delta(x) U^{e\prime}(x) f$ transforms the second-order system of PDEs (3ab) into the single third-order Falkner-Skan ODE

$$f''' + f f'' + \beta\left(1 - f'^2\right) = 0 \qquad (4)$$

with boundary conditions $f(0) = f'(0) = 0$; $f'(\infty) = 1$, provided that the outer velocity $U^e(x)$ is a suitable power law of the x-coordinate. The corresponding thickness scale is

$$\Delta(x) = \sqrt{\frac{(2 - \beta)\nu x}{U^e(x)}} \qquad (5)$$

Equation (4) is much simpler to solve that (3ab), using a Runge-Kutta method for instance. Moreover, the similarity solution $f(\eta)$ is entirely driven by the geometrical parameter β and is independent of the Reynolds number: it can be solved once for all, and the physical solution comes through the change in variables. Now, the question is to find the power law for $U^e(x)$ (needed for boundary layer self-similarity) associated to a given angle $\beta \frac{\pi}{2}$ of the wedge. Classically, this is obtained by inviscid potential flow theory and conformal mapping: the slip

velocity at the wall of the potential flow serves as outer velocity (U^e) for the boundary layer.

Let $\Phi(Z) = kZ$ be the complex potential of a uniform flow of arbitrary velocity k on the upper-half complex plane $\mathrm{Im}(Z) > 0$, Z being the complex coordinate (Fig. 4). The open Schwartz-Christoffel transformation $z = H(Z) = Z^{1/n}$ makes a conformal mapping onto the z physical plane in which the potential is $\phi(z) = \Phi(Z) = kz^n$. The complex velocity $w(z) = \dfrac{d\phi}{dz} = u - iv = nkz^{n-1}$ gives the slip velocity on the wall $\mathrm{Re}\{z\} = x > 0 : U^e(x) = nkx^{n-1}$. Now we have the simple geometrical relation $\beta\dfrac{\pi}{2} = \pi - \dfrac{\pi}{n}$ from which the final expression for the searched velocity distribution comes out:

$$U^e(x) = \frac{2k}{2-\beta}\, x^{\frac{\beta}{2-\beta}} \qquad (6)$$

Figure 4

Equation (6) appeals some comments: the case $\beta = 0$ reproduces the standard Blasius flat-plate problem $U^e(x) = k = U_\infty = cst$ for which the thickness-scale $\Delta(x)$ is a square-root function of x. The case $\beta = 1$ corresponds to the stagnation point flow described on Fig 3A of Prieto & al. (1996), with constant thickness-scale $\Delta(x) = \sqrt{\nu/k}$ depending on the arbitrary value of k. For $\beta \in]0,1]$, the potential flow, hence the outer velocity $U^e(x)$ takes infinite values as $|x| \to \infty$ and vanishes at the apex of the crystal face. This is physically irrelevant: the physical condition at infinity (far from the crystal) is $U_\infty = cst$. For negative values of β (the limiting case $\beta = -0.199$ (angle –18°) corresponds to a vanishing wall shear stress $f''(0) = 0$ hence to flow separation), the flow is at rest at infinity, accelerates to reach infinite values at the apex and then

decelerates again along the crystal face. Does it mean that the theory is useless? No, simply the potential law (6) is only valid in the neighbourhood of the apex. Hence, in the general case of figure 4, one has to find the range of x for which (6) applies and to derive the corresponding value $k(U_\infty, \beta)$. This can be done using the FLUENT V6.2 computational fluid dynamics software to solve the Navier-Stokes equations under the assumption of inviscid fluid (but not potential flow), i.e. incompressible Euler equations. The computed slipping velocities at the crystal surface are compared to (6), and $k(U_\infty, \beta)$ is estimated (Fig. 5 and, Table 1). The parametric study has been performed for β variable from 1 to -0.199 and U_∞ from 0.001 ms^{-1} to 5 ms^{-1} (Table 1). Results show that $k(U_\infty,\beta)$ increases linearly with U_∞ and exponentially with β:

$$k(U_\infty, \beta) \approx 1.4U_\infty(1.17 - \beta)^{-2.8} \qquad (7)$$

Figure 5

Table 1

Now, the solution $f(\eta)$ of (4), together with (5), (6) and (7) solves completely the flow problem (3ab) which is at disposal for the concentration equation (3c).

4 DEFINITION OF THE LOCAL DIFFUSION THICKNESS $\Delta_c(x)$

First, we are looking for the concentration profile $c(x, y)$ which varies from c_∞ in the free stream down to c_w at the crystal wall. Since the hydrodynamic boundary layer is self-similar and eq. (3c) is linear, it appears that the concentration boundary layer is also self-similar: the change in variable $c(x, y) = c_w + (c_\infty - c_w)\chi_\beta(\eta)$ transforms the PDE (3c) into the following ODE equipped with simple boundary conditions, and easy to solve, given any $f(\eta)$ associated to a value β in (4)

$$\chi_\beta'' + S_c \chi_\beta' f = 0 \qquad \chi_\beta(0) = 0 \quad ; \quad \chi_\beta(\infty) = 1 \tag{8}$$

In χ_β, the underscore β emphasizes on the dependence of the concentration profile on the geometrical parameter β. From (4) and (8), self similar velocity and concentration profiles can be calculated for various β (Figs 6a and 6b). The concentration profile varies sharply with increasing the Schmidt number (Fig. 6c).

Figure 6

In order to define a diffusion thickness suitable for the growth rate calculation, it is necessary to link Δ_c to the mass flux at the crystal wall (i.e. y=0; Fig.7)

$$J_w(x) = -D \left.\frac{\partial c}{\partial y}\right|_{y=0} = -D(c_\infty - c_w) \frac{\chi_\beta'(0)}{\Delta(x)} \tag{9}$$

which may be non-dimensionalized as a local Nusselt number

$$Nu(x) = J_w(x) \frac{x}{D(c_\infty - c_w)} = -x \frac{\chi_\beta'(0)}{\Delta(x)} \tag{10}$$

Now, we introduce the diffusion thickness, defined geometrically as (Fig. 7)

$$\Delta_c(x) = \frac{(c_\infty - c_w)}{\left.\frac{\partial c}{\partial y}\right|_{y=0}} \tag{11}$$

which reads also simply $\Delta_c(x) = -\frac{x}{Nu(x)} = \frac{\Delta(x)}{\chi_\beta'(0)}$ or in full:

$$\Delta_c(x) = x^{\frac{1-\beta}{2-\beta}} \sqrt{\frac{\nu}{2k(U_\infty, \beta)}} \frac{2-\beta}{\chi_\beta'(0)} \tag{12}$$

Figure 7

5 DISCUSSION ON THE PARAMETERS GOVERNING THE GROWTH RATE

Equation (2) shows that the surrounding flow influences the crystal growth rate through the diffusion thickness. Using the model proposed to estimate $\Delta_c(x)$, the local growth rate reads:

$$R_x = \frac{N_0 \Omega D_{v.dif} \sigma}{\sqrt{\frac{\nu}{2k(U_\infty, \beta)}} \frac{2-\beta}{\chi_\beta'(0)}} x^{-\frac{1-\beta}{2-\beta}} \qquad (13)$$

Garside *et al.* (1975) observed that bulk growth is proportional to square root of the flow velocity and Hilgers & Urai (2002) suggested a formulation proportional to $U_\infty^{0.3}$. As the parameter $k(U_\infty,\beta)$ is a linear function of flow kinetics, the expression of the local growth rate (13) is in good agreement with the observation of Garside *et al.* (1975) on bulk crystal shape.

This local growth rate depends on geometrical parameters: β and x. A particular value is β=1, for which the growth rate doesn't depend on x, and the diffusion thickness depends only on the fluid velocity. In any other case β<1, the value $\Delta_c(x)$ increases with x. The constant diffusion thickness $\Delta_\perp$ for faces normal to the flow will be used to normalize relative growth rates (§ 6, eq. (16)) and is given by:

$$\Delta_\perp = \sqrt{\frac{\nu}{2\ k(U_\infty,1)}} \frac{1}{\chi_\perp'(0)} \qquad (14)$$

Near the apex, the present model is questionable because $\mathrm{Re}_x \approx 1$ and Prandtl equations (3ab) are no more valid. At the limit $x \to 0$, the model is singular. It is then possible to define roughly a critical value x_c such that for $0 < x < x_c$ wall fluxes are very high and surface processes dominate in (1), and for $x_c < x$, the growth is driven by volume diffusion (to which the present model applies).

Figure 8

Now, depending on the value of x_c, three types of bulk growth can be considered (Fig. 8):

- First, when x_c is small, very high growth rates localized on the edges in the apex area suggest that crystal should develop dendritic shapes.
- Second, for intermediate values of x_c, the growth rate decreases with x, the trend in β is not obvious due to the combination of (6) in the hydrodynamic model and the empirical power law in (7).
- Finally, for higher values of x_c, the growth rate increases with β and still decreases with x, i.e. growth is higher in the upstream direction and decreases downstream.

This discussion states that when the crystals are small, the faces exposed at high angle with respect to the flow direction are not necessarily those with the highest growth rate. Moreover, the always decreasing growth rate with x explains the occurrence of concave curved shape faces as observed in the Chaudes-Aigues pipe (e.g. Sizaret *et al.* 2006 Fig. 1e in Part I).

6 TEXTURE RECONSTRUCTION

In this part, the model is applied to the reconstruction of the texture observed on the calcites formed in a pipe at Chaudes-Aigues. Calcite crystallises in a flow of constant direction (the pipe) and constant temperature of about 70°C (Sizaret *et al.* 2006, Part I). The following discussion assumes that crystals behave independently, i.e. concentration boundary layers occurring on a crystal do not influence each others. This assumption is well verified for high Schmidt numbers (Fig. 6c) or for high flow velocity, when the boundary layer is thin and do not separate.

The textural study in Part I (Sizaret *et al.* 2006, Fig. 1d in Part I) suggests that the calcite

crystal has its <c> axis in vertical position rising in the flowing solution. Therefore, reconstruction focuses on a horizontal plane, i.e. the section normal to <c> with trigonal symmetry. Absolute reconstruction with (13) is not obvious since parameters N_0 and Ω of eq. (1) are not well known. So, in this part, we reconstruct the shape using the relative growth of different faces. From (2), when diffusion dominates, it is easy to show that the local ratio of growth band thicknesses $L_1(x)/L_2(x)$ of two faces 1 and 2 is equal to the inverse of the local diffusion thicknesses ratio:

$$\frac{L_1(x)}{L_2(x)} = \frac{\Delta_{2c}(x)}{\Delta_{1c}(x)} \tag{15}$$

As mentioned above, the diffusion thickness (14) is constant for normal faces (β=1). It is then obvious to normalise all the growth bands thicknesses with $L_\perp$. With (12) and (14), eq. (15) reads:

$$\frac{L(x)}{L_\perp} = \frac{\chi_\beta'(0)}{\chi_\perp'(0)} \sqrt{\frac{k(U_\infty,\beta)}{k(U_\infty,1)}} \frac{x^{-\frac{1-\beta}{2-\beta}}}{2-\beta} \tag{16}$$

This latter expression is independent of U_∞ because equation (7) for $k(U_\infty,\beta)$ is a linear function of U_∞. Diffusion coefficients of Ca^{2+} and CO_3^{2-} are about 1.5 10^{-9} m^2s^{-1} (Vanysek 2001), and dynamic viscosity at 70°C is close to 0.4 10^{-6} m^2s^{-1} (Haar *et al.* 1984). The Schmidt number in (8) is then estimated at about 260. From the numerical solution of (8), the $\chi_\beta'(0)$ function has been approximated by:

$$\chi'_\beta(0) \approx 4.1(0.1995+\beta)^{1/6} \quad ; \quad \mathrm{Sc} = 260 \tag{17}$$

The flow velocity within the pipe is estimated at about 0.01 ms^{-1} and the length of crystals faces range between 100 (Re_x=3.4) and 200 µm (Re_x=6.6), thus the assumption $\sqrt{Re_x} >> 1$ is not well

verified and the model is not accurate, but still provides a framework to interpret the observed anisotropy in mineral textures.

Successive bands are reconstructed in three steps, on an initially isotropic shape with faces about 100 μm long (Fig. 9). In order to obtain a ≈200 μm shape, $L_{\perp}$ has been taken quite arbitrarily to be 37.5 μm.

The reconstruction of growth bands needs flat edges, but the growth rate formulation (13) produces curved shapes. In order to make the reconstruction possible at each step, we approximate the curve resulting from (16) by its tangent at the end of the edge where x and Re_x have maximum values (Fig. 9). A consequence for this approximation is to lower the degree of anisotropy of the final shape. The growth rate of the downstream face has also to be estimated because no mathematical expression can be found for β <-0.199. Low chemical fluxes in shade area may be due to the influence of upstream faces that consume the elements in the solution, hence lower the concentration in the hydrodynamic wake of the crystal. Low growth rates in this area have been confirmed by experiments on ADP (Prieto *et al.* 1996) and observations in calcites (e.g. Sizaret *et al.* 2006, Fig. 4b in Part I). Therefore, in our reconstruction, growth bands on faces in downstream position have thicknesses (noted L_s on Fig.9) equal to the lower calculated value along upstream faces.

Figure 9

Figure 10 presents the three steps of crystal growth in the (0001) plan. In this example the crystal faces having the lower angle with respect to the flow direction have the higher growth rate and *vice-versa* (Fig. 10e). This is in good agreement with observed growth bands on small

crystals (Fig. 4b in Part I). The initial shape has a trigonal symmetry. The model that predicts higher upstream local growth rates produces elongated shapes. Initial crystals with a plane of symmetry parallel to the flow direction will develop elongated shapes that preserve the initial plane of symmetry, as predicted by the Curie principle (Fig. 10b). When crystals are randomly oriented, the long axis rotates towards the flow direction (Figs 10c-10f). This is in good agreement with the two sub populations observed in the Chaudes-Aigues calcite (Figs 1f and 1i in Part I).

Figure 10

7 CONCLUSIONS

In this paper, an original model is proposed to predict crystal growth rates when volume diffusion dominates. This hydrodynamic model of diffusion through boundary layers allows to derive an analytically equation for the local growth rate along a crystal face. The main parameter controlling the final crystal shape is the angle between the face and flow direction. The growth rate decreases downstream along the faces and modifies the crystal wall orientation. This behaviour explains the formation of elongated shapes with slight deviation with respect to the flow direction.

The reconstructions performed on randomly oriented initially trigonal shapes are in a good agreement with observations and measurements performed on natural calcite crystallization presented in Part I of this study. The predictability of the model is limited by the assumption that other crystals have negligible influence and by low local Reynolds numbers, which falls beyond the classical boundary layer theory. More precise predictions could be obtained from Navier-Stokes simulations, feasible with nowadays computers. Nevertheless, this work has enlighten the

main physical parameters that drive crystal growth rates in flowing solutions, and is useful to interpret observed natural mineral textures.

ACKNOWLEDGEMENTS

Our grateful acknowledgements go to Florent SEDALO and, Jeremy CAILLET (Ecole Polytechnique de l'Université d'Orléans) who performed hydrodynamic simulations . We thank Dr H. Schmeling and anonymous reviewer for theirs fruitfull criticisms which helped us to improve the original manuscript. We thank also the French REGION CENTRE for financial support during the post doctoral research for the first author.

REFERENCES

Burton, W.K., Cabrera, N. & Frank, F.C., 1951. The growth of crystals and the equilibrium structure of their surfaces, *Phil Trans Roy Soc London*, A243, 243-299.

Carlson, A., 1958. The fluid mechanics of crystal growth from solution, *in Growth and perfection of crystals*, pp. 421--426, ed. R.H. Doremus, B.W. Roberts, and D. Turnbull , Wiley and sons, New York.

Chernov, A.A., 1992. How does the flow within the boundary layer influence morphological stability of a vicinal face? *J. Crystal Growth*, 118, 333-347.

Chernov, A.A., 2004. Notes on interface growth kinetics 50 years after Burton, Cabrera and Frank. *J. Crystal Growth*, 264, 499-518.

Curie, P., 1908. *Œuvres*, 118p Gautier-Villars, Paris, Société Française de Physique. Reprinted : Archives contemporaines, Paris 1984.

Evans, H.L., 1961. Mass transfer through laminar boundary layers-3a. similar solutions of b-equation when b=0 and $\sigma \geq 0.5$. *Int. J. Heat Mass Transfer*, 3, 26-41.

Fluent 5.0, User's guide, Fluent inc., Canterra Resource Park, 10 Cavendish Court, Lebanon NH 03766, USA, Vol. 3.

Garside, J., Janssen-van Rosmalen, R. & Bennema, P., 1975. Verification of crystal growth rate equations. *J. Crystal Growth*, 29, 353-366.

Gilmer, G.H., Chez, R. & Cabrera N., 1971. An analysis of combined surface and volume diffusion processes in crystal growth. *J. Crystal growth*, 8 79-93.

Haar, L., Gallagher, J.S. & Kell, G.S., 1984. *NBS/NCR Steam Tables*, pp. 320, Hemisphere Publishing Corporation, New York

Hilgers, C. & Urai, J.L., 2002. Experimental study of syntaxial vein growth during lateral fluid flow in transmitted light: first results. *J. Str. Geol.*, 24, 1029-1043.

Kessler, S.E., Stoiber, R.E. & Billings, G.K., 1972.Direction of flow mineralizing solutions at Pine Point, N. W. T. *Econ. Geol.*, 67, 19-24.

Kostov, I. & Kostov, R.I., 1999. Crystal Habits of Minerals, 415 pp. Pensilvania, Sofia,.

Lebedev, L.M., 1967. Metacolloid in Endogenic Deposits, 298 pp. Plenum Press, New York.

Prieto, M. & Amoros, J.L., 1981. On the influence of hydrodynamic environment on crystal growth. *Bull. Minéral.*, 104, 114-119.

Prieto, M., Paniagua, A. & Marcos, C., 1996. Foramtion of primary inclusions under influence of the hydrodynamic environment. *Eur. J. Mineral.*, 8, 987-996.

Rosenberger, F., 1979. *Fundamentals of crystal growth I. Macroscopic equilibrium and transport concepts*, pp. 215-394, ed. Cardona, M., Fulde, P. & Queisser, HJ., Springer Series in Solid-State Sciences 5, Springer-Verglag, Berlin Heidelberg New York

Schlichting H., 1968. *Boundary-layer Theory*, 6th edn, pp. 77-310 Mc Graw-Hill book company.

Sizaret, S., Chen, Y., Barbanson, L., Marcoux, E., 2006. Crystallisation in flow Part I: track paleo-circulation by texture analysis, and magnetic fabrics, accepted.

Vanysek, P., 2001. Ionic conductivity and diffusion at infinite dilution, in: *Handbook of chemistry and physics*, 81st edn, pp. 595-597 ed. D.R. Lide, Boca Raton, New York, London.

FIGURE AND TABLE CAPTIONS

Figure 1**.** The three stages of crystal growth related to the quantitative parameters defined by Gilmer *et al.* (1971). See text for details: (i) volume diffusion, (ii) incorporation in the adsorbed layer (V_{ads}: velocity of adsorption on crystal surface), (iii) surface diffusion and incorporation in the crystal (V_{kink}: velocity of incorporation of adsorbed molecules in kink sites).

Figure 2. Velocity and concentration profiles used to define hydrodynamic and concentration boundary layers; A: apex, see text for parameters definitions.

Figure 3. Self-similar flow velocity profiles along a crystal wall (wedge); see text for parameters definitions.

Figure 4. Schwartz-Christoffel transformation making a conformal mapping of the upper half complex plane; see text for parameters definitions.

Figure 5. Diagram comparing the velocity profile along the wedge wall calculated with FluentV6.2 code (grey line) and the curve given by the potential law (black line). This comparison shows a good agreement for length less than 0.0015 m (dotted line). Moreover these curves allow to estimate k at different β and U_∞, the presented case is for $\beta = 45°$ and $U_\infty = 0.02$ ms^{-1}. In the box it is presented the geometry of the simulation.

Figure 6. Self-similar profiles. (a) Velocity profiles as functions of the geometrical parameter β corresponding to wedge angles of -18° (flow separation), 0°, 45° and 90° (stagnation point).

Concentration profiles: (b) corresponding to velocity profiles for unit Schmidt number (Sc=1) and (c) for flat plate (β=0) as a function of Schmidt number S_c= 1, 10, 10^2, 10^3 and 10^4.

Figure 7. The concentration profile defines the local diffusion thickness $\Delta_c(x)$ along crystal wall. Dotted lines represent the limit of the boundary layer, see text for parameters definitions.

Figure 8. Growth rate for faces with different orientations with respect to the flow (0.01 ms^{-1}). x_c is the critical length where the crystal growth changes from surface to volume diffusion processes. When surface processes dominate, the growth rate does not depend on x and can be assumed constant.

Figure 9. First step of the crystal growth reconstruction (see text for details).

Figure 10. Schematic reconstruction of 3 stages of calcite growth in a flowing solution, the view is given in the (0001) plane that is perpendicular to the <c> axis. (a) Isotropic initial shape; (b) the flow is parallel to the symmetry plane of the crystal; (c) to (f) reconstruction of crystal growth for faces making angles with flow varying from 30° to –10° (associate faces has angles from 30 to 70). The long axis of the elongated shape (grey line) is modelled with the SPO program and statistics shows an average angle of 19° with the flow direction. By symmetry, it is obvious that the texture presents two sub populations slightly deviated with respect to flow direction (19° and –19°) as observed in Chaudes-Aigues pipe (Sizaret *et al.* 2006, Part I).

Table 1. Dependence of $k(U_\infty, \beta)$ on U_∞ and β.

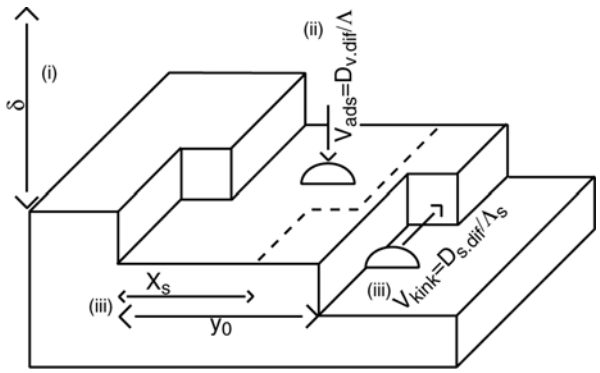

Figure 1**.** The three stages of crystal growth related to the quantitative parameters defined by Gilmer *et al.* (1971) see text for details: (i) volume diffusion, (ii) incorporation in the adsorbed layer (V_{ads}: velocity of adsorption on crystal surface), (iii) surface diffusion and incorporation in the crystal (V_{kink}: velocity of incorporation of adsorbed molecules in kink sites).

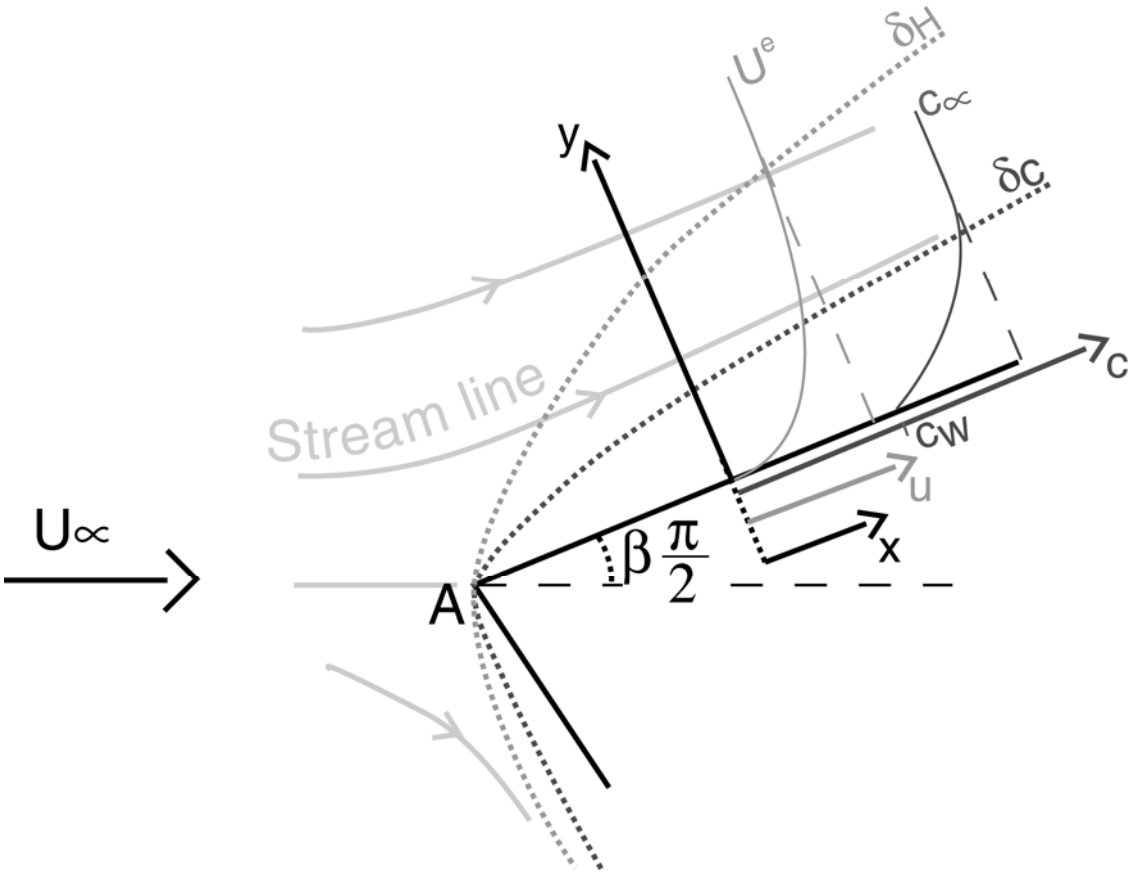

Figure 2. Velocity and concentration profiles used to define hydrodynamic and concentration boundary layers; A: apex, see text for parameters definitions.

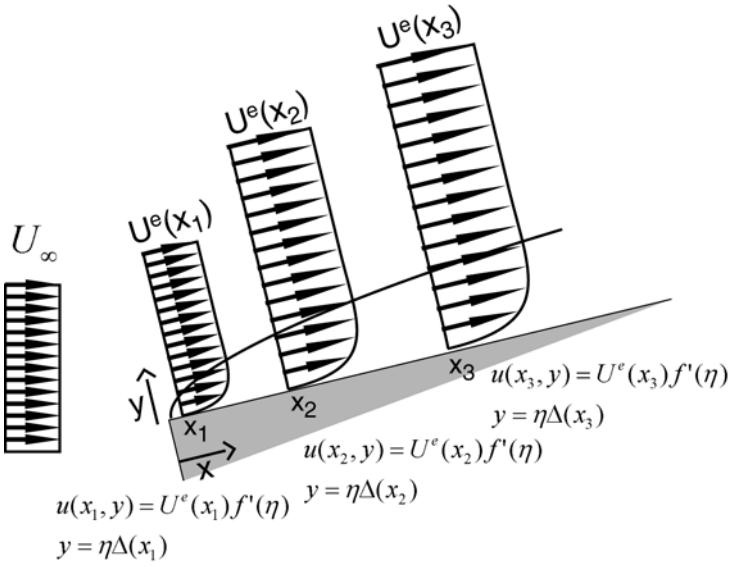

Figure 3. Self-similar flow velocity profiles along a crystal wall (wedge); see text for parameters definitions.

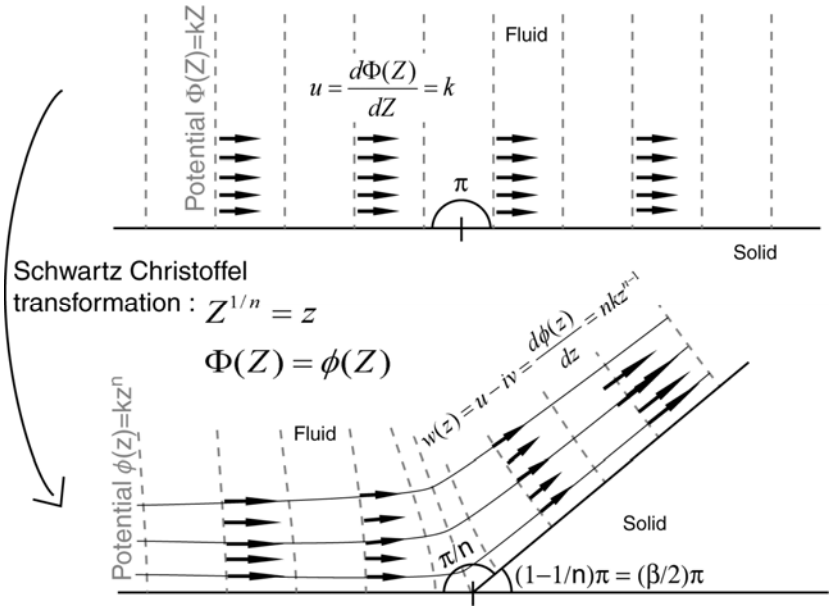

Figure 4. Schwartz-Christoffel transformation making a conformal mapping of the upper half complex plane; see text for parameters definitions.

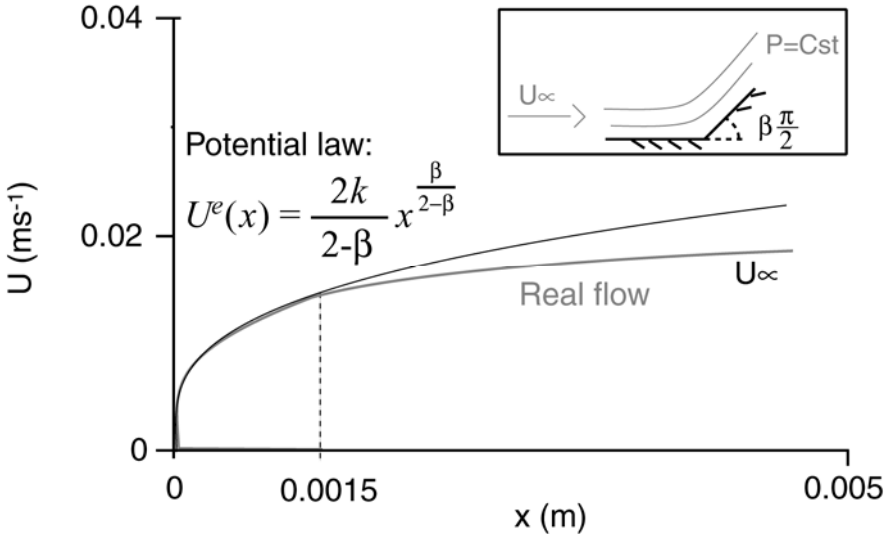

Figure 5. Diagram comparing the velocity profile along the wedge wall calculated with FluentV6.2 code (grey line) and the curve given by the potential law (black line). This comparison shows a good agreement for length less than 0.0015 m (dotted line). Moreover these curves allow to estimate k at different β and U_∞, the presented case is for $\beta = 45°$ and $U_\infty = 0.02$ ms^{-1}. In the box it is presented the geometry of the simulation.

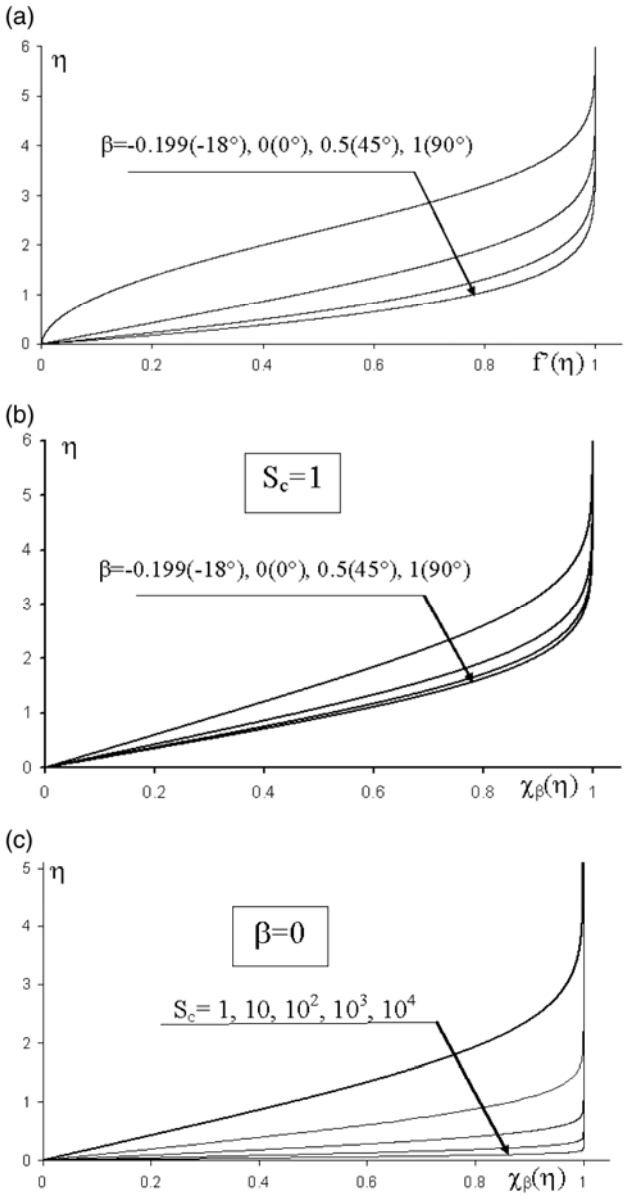

Figure 6. Self-similar profiles. (a) Velocity profiles as functions of the geometrical parameter β corresponding to wedge angles of -18° (flow separation), 0°, 45° and 90° (stagnation point). Concentration profiles: (b) corresponding to velocity profiles for unit Schmidt number (Sc=1) and (c) for flat plate (β=0) as a function of Schmidt number S_c= 1, 10, 10^2, 10^3 and 10^4.

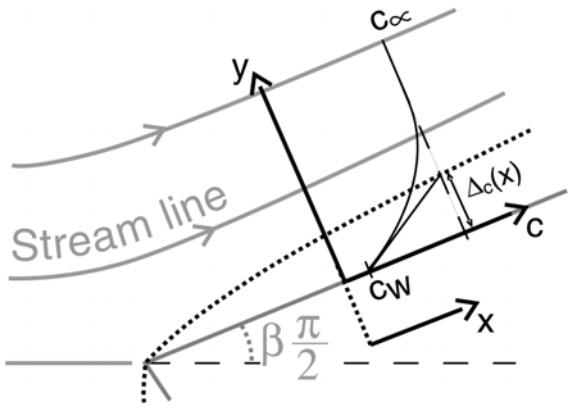

Figure 7. The concentration profile defines the local diffusion thickness $\Delta_c(x)$ along crystal wall.

Dotted lines represent the limit of the boundary layer, see text for parameters definitions.

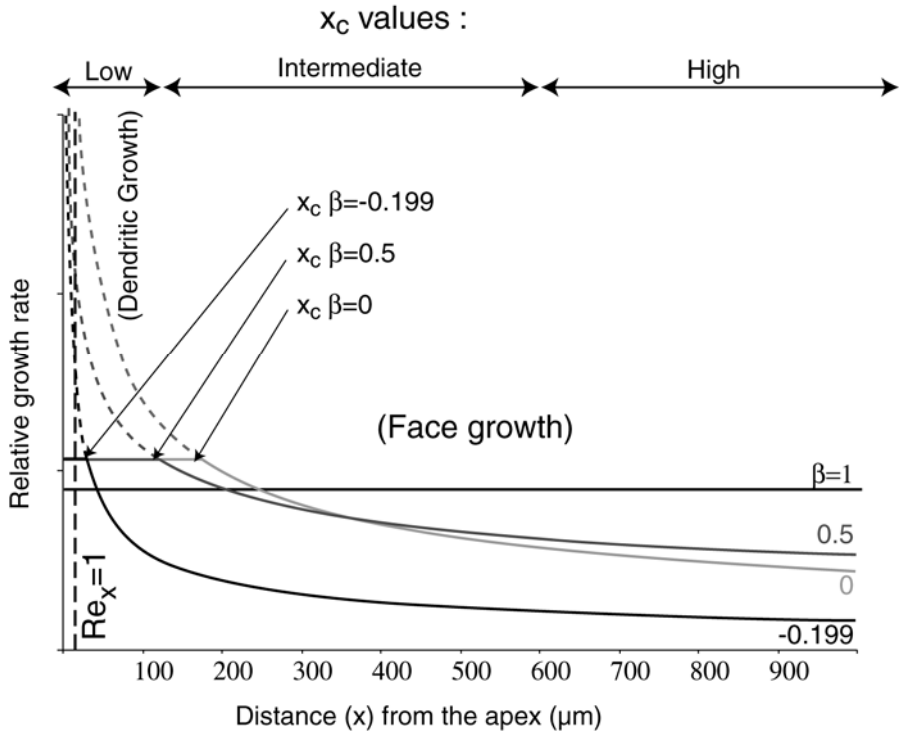

Figure 8. Growth rate for faces with different orientations with respect to the flow (0.01 ms^{-1}). x_c is the critical length where the crystal growth changes from surface to volume diffusion processes. When surface processes dominate, the growth rate does not depend on x and can be assumed constant.

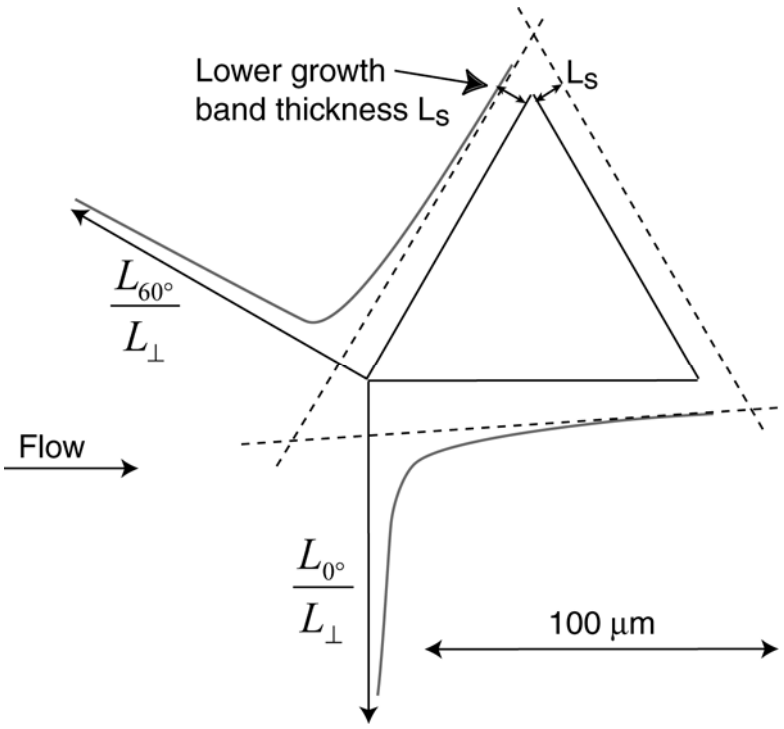

Figure 9. First step of the crystal growth reconstruction (see text for details).

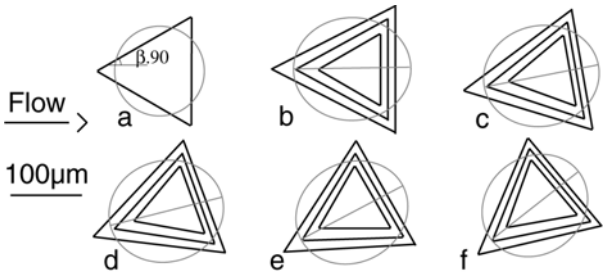

Figure 10. Schematic reconstruction of 3 stages of calcite growth in a flowing solution, the view is given in the (0001) plane that is perpendicular to the <c> axis. (a) Isotropic initial shape; (b) the flow is parallel to the symmetry plane of the crystal; (c) to (f) reconstruction of crystal growth for faces making angles with flow varying from 30° to –10° (associate faces has angles from 30 to 70). The long axis of the elongated shape (grey line) is modelled with the SPO program and statistics shows an average angle of 19° with the flow direction. By symmetry, it is obvious that the texture presents two sub populations slightly deviated with respect to flow direction (19° and –19°) as observed in Chaudes-Aigues pipe (Sizaret *et al.* 2006, Part I).

Table 1. Dependence of $k(U_\infty, \beta)$ on U_∞ and β.

$k(U_\infty,\beta)$	$\beta\pi/2$ (°)											
	-18	-10	0	10	20	30	40	50	60	70	80	90
0	0	0	0	0	0	0	0	0	0	0	0	0
0.005	0.0031	0.0038	0.005	0.0068	0.01	0.014	0.0222	0.04	0.07	0.15	0.379	1.054
0.01	0.0062	0.0076	0.01	0.0135	0.019	0.028	0.0439	0.07	0.14	0.3	0.75	2.104
0.05	0.0310	0.0379	0.05	0.0675	0.095	0.14	0.2190	0.35	0.7	1.5	3.77	10.376
0.1	0.0621	0.0759	0.1	0.135	0.19	0.28	0.441	0.75	1.4	3	7.6	20.748
0.5	0.3105	0.3790	0.5	0.675	0.98	1.41	2.210	3.7	7	15	37.5	103.76
1	0.6200	0.7600	1	1.35	1.9	2.8	4.415	7.2	14	30	74.8	207.52
5	3.1100	3.8000	5	6.75	9.5	14	21.950	36	69	150	379	1037.6

U_∞ (ms^{-1})

*****

Appendix: Figures 1 and 4, in Part I.

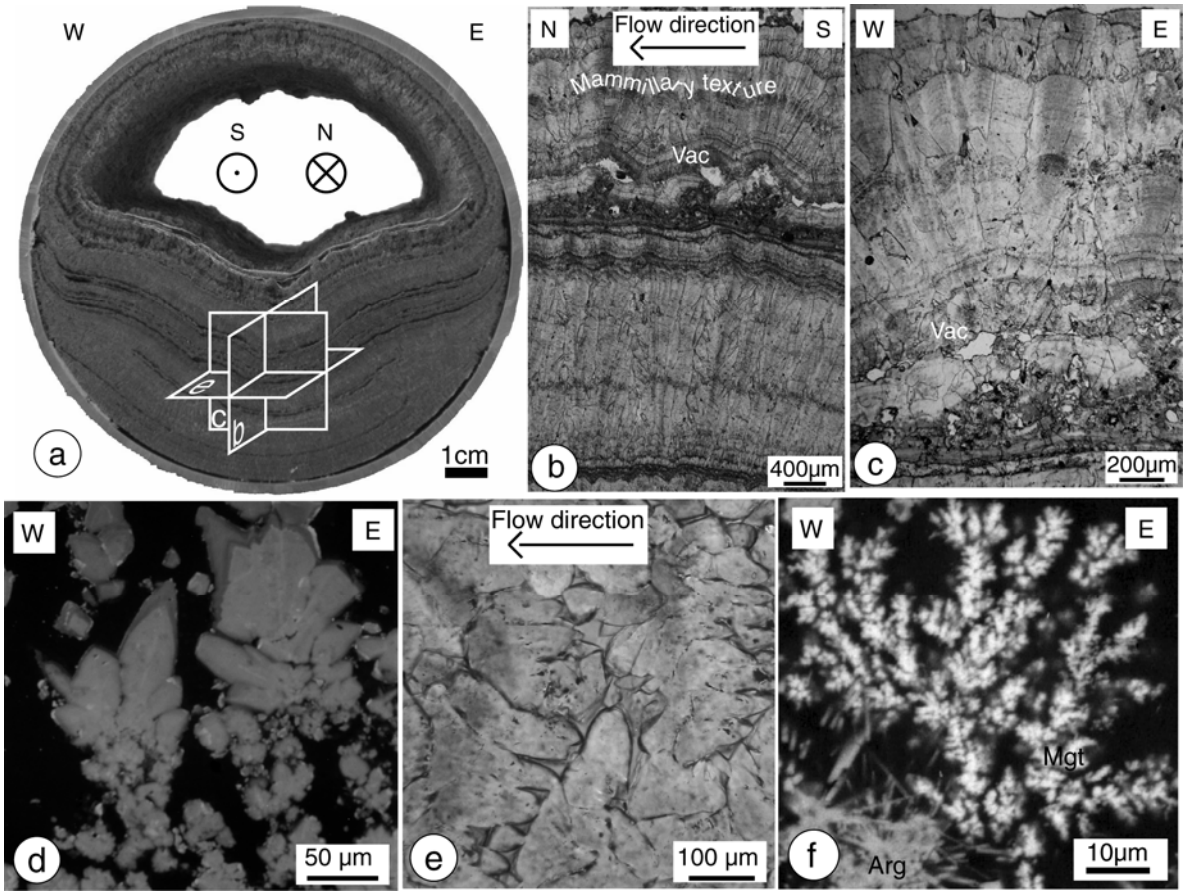

Figure 1. Precipitates in the Chaudes-Aigues horizontal pipe. (a) Pipe section showing calcite bands; (b) Radiating sheaf texture vertical and parallel to the pipe axis. Vac = vacuole; (c) Sheaf textures observed in the vertical section of the pipe; (d) Crystal of the last calcite band rising in the flowing solution (Cathodoluminescense); (e) Calcite textures in the plane horizontal with elongated shapes; (f) Electron back-scattering image of a vertical section (SEM) showing aragonite (Arg) and dendrites of magnetite (Mgt);

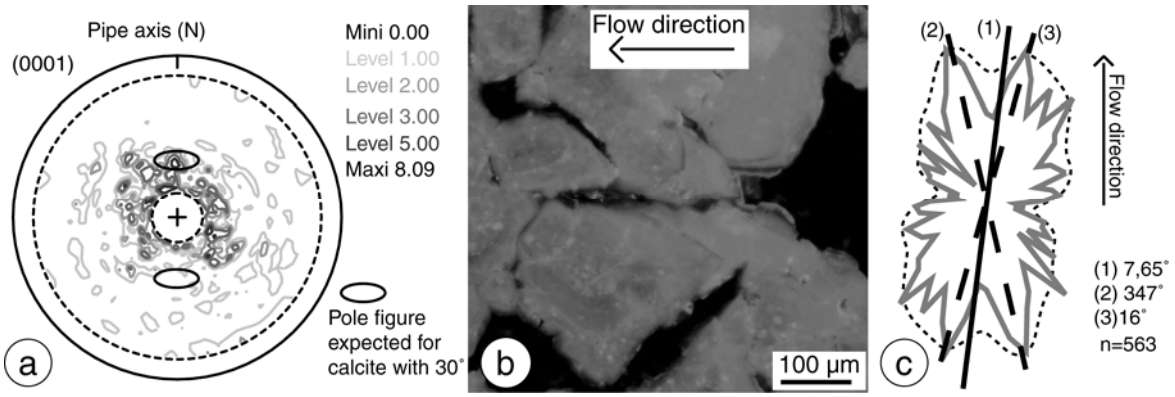

Figure 4. Analysis of the calcite texture. (a) Lattice preferred orientation of the (0001) pole plane i.e. the calcite <c> axis, the grey levels indicate the diffracted X-ray intensities; (b) Growth bands in calcite section cut in the horizontal plane (Cathodoluminescense); (c) Distribution of the calcite long axes in the plane normal to the <c> axis. These statistics have been performed on a thin section of 3.5 x 2.5 mm^2.